LEVEL

A TRIDENT SCHOLAR
PROJECT REPORT

NO. 106

BASIC STUDIES OF A FLOURINE
ANION SUPERIONIC CONDUCTOR

DTIC
ELE
NOV 1 4 1980
C

UNITED STATES NAVAL ACADEMY
ANNAPOLIS, MARYLAND
1980

80 11 7 124
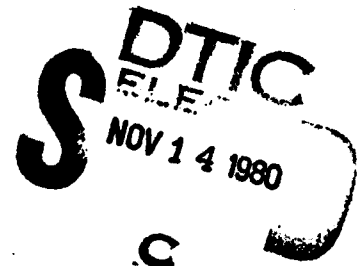
REPORT DOCUMENTATION PAGE		READ INSTRUCTIONS BEFORE COMPLETING FORM
1. REPORT NUMBER U.S.N.A. - TSPR; no. 106 (1980)	2. GOVT ACCESSION NO. AD-A091 702	3. RECIPIENT'S CATALOG NUMBER
4. TITLE (and Subtitle) BASIC STUDIES OF A FLUORINE ANION SUPERIONIC CONDUCTOR		5. TYPE OF REPORT & PERIOD COVERED Final: 1979/1980
		6. PERFORMING ORG. REPORT NUMBER
7. AUTHOR(s) John Reeves/Igel		8. CONTRACT OR GRANT NUMBER(s)
9. PERFORMING ORGANIZATION NAME AND ADDRESS United States Naval Academy, Annapolis.		10. PROGRAM ELEMENT, PROJECT, TASK AREA & WORK UNIT NUMBERS
11. CONTROLLING OFFICE NAME AND ADDRESS United States Naval Academy, Annapolis.		12. REPORT DATE 5 June 1980
		13. NUMBER OF PAGES 53
14. MONITORING AGENCY NAME & ADDRESS(if different from Controlling Office)		15. SECURITY CLASS. (of this report) UNCLASSIFIED
		15a. DECLASSIFICATION/DOWNGRADING SCHEDULE

16. DISTRIBUTION STATEMENT (of this Report)

This document has been approved for public release;
its distribution is UNLIMITED.

17. DISTRIBUTION STATEMENT (of the abstract entered in Block 20, if different from Report)

This document has been approved for public release;
its distribution is UNLIMITED.

18. SUPPLEMENTARY NOTES

Accepted by the U.S. Trident Scholar Committee.

19. KEY WORDS (Continue on reverse side if necessary and identify by block number)

Fluorine
Superionic conductors
Anions
Dielectric relaxation
Lanthanum trifluoride

20. ABSTRACT (Continue on reverse side if necessary and identify by block number)

Audio frequency conductivity and capacitance measurements in the temperature range of 5.4-310K have been used to study the conductivity and dipolar relaxation phenomena in calcium doped lanthanum trifluoride. Measurements have been taken at five frequencies from 100 Hz to 10 kHz on samples varying in concentration from 0.01% to 0.3%. one strong dipolar dielectric relaxation and several weaker relaxations have been observed both parallel and perpendicular to the c-axis. The strong dipolar relaxation has been attributed to the re-
OVER !

DD FORM 1473 EDITION OF 1 NOV 65 IS OBSOLETE
1 JAN 73
S/N 0102-LF-014-6601

20.

CONTINUED

alignment of a charge compensating fluorine ion vacancy about a substitutional alkaline-earth ion. The weaker relaxations have been attributed to trace impurities because of the lack of any regular progression in either concentration or direction of applied field. Measurements indicate that, for samples of similar concentrations, the strength of the dipolar dielectric relaxation perpendicular to the c-axis is from 1.5-1.9 times the strength parallel to the c-axis. This has been attributed to a dipole moment perpendicular to the c-axis which is significantly greater than that parallel to the c-axis. An activation enthalpy in the dipolar region of $.31 \pm .03$ eV has not been observed. At higher temperatures, a thermally activated or association region has been observed. An activation enthalpy for this region of $.49 \pm .03$ eV and an association energy of $.38 \pm .03$ eV is reported.

0 - 0

S/N 0102- LF- 014- 6601

BASIC STUDIES OF A FLUORINE
ANION SUPERIONIC CONDUCTOR
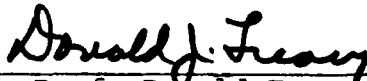
A Trident Scholar Project Report

by

Midshipman John R. Igel, Class of 1980

U. S. Naval Academy

Annapolis, Maryland

Assoc. Prof. John Fontanella
Physics Department

Prof. Donald Treacy
Physics Department

Accepted for Trident Scholar Committee

Chairman

---

5 June 1980

Date

ABSTRACT

Audio frequency conductivity and capacitance measurements in the temperature range of 5.4-310K have been used to study the conductivity and dipolar relaxation phenomena in calcium doped lanthanum trifluoride. Measurements have been taken at five frequencies from 100 Hz to 10 kHz on samples varying in concentration from 0.01% to 0.3%. One strong dipolar dielectric relaxation and several weaker relaxations have been observed both parallel and perpendicular to the c-axis. The strong dipolar relaxation has been attributed to the realignment of a charge compensating fluorine ion vacancy about a substitutional alkaline-earth ion. The weaker relaxations have been attributed to trace impurities because of the lack of any regular progression in either concentration or direction of applied field. Measurements indicate that, for samples of similar concentrations, the strength of the dipolar dielectric relaxation perpendicular to the c-axis is from 1.5-1.9 times the strength parallel to the c-axis. This has been attributed to a dipole moment perpendicular to the c-axis which is significantly greater than that parallel to the c-axis. An activation enthalpy in the dipolar region of $.31 \pm .03$ eV has been observed. At higher temperatures, a thermally

1

activated or association region has been observed. An activation enthalpy for this region of .49+.03 eV and an association energy of .38+.03 eV is reported.

ACKNOWLEDGEMENTS

TABLE OF CONTENTS

INDEX TO FIGURES AND TABLES

Tables   Page

INTRODUCTION

The study of superionic or fast ion conductors has become increasingly intense in recent years. A superionic conductor is a term applied to a general class of solid materials which exhibit ionic conductivities as high as those of aqueous solutions or ionic melts. Studies of these materials are important not only for the information they yield about solids in general, but also from the standpoint of the possible application of superionic conductors to solid state batteries. Solid state batteries are high energy density voltaic cells which use solid electrolytes (i.e. superionic conductors) instead of the liquid electrolyte currently being used. Of those materials currently being investigated as possible fast ion conductors, fluorides have attracted attention because some fluorides are known to be good fluorine anion conductors[1]. Rare-earth fluorides (e.g. lanthanum trifluoride, LaF_3) are of this type.

LaF_3 has already been the subject of many experiments. Among the experimental techniques used have been: electrical conductivity [1,2,3], nuclear magnetic resonance of F^{19} [1,2], dielectric relaxation [4], ionic thermocurrent [3], and thermal conductivity [5]. This research uses both dielectric relaxation and electrical conductivity techniques.

To date, most studies of LaF_3 have been concerned with the pure compound. The system of LaF_3 doped with barium has also been studied [6]. This study dealt with LaF_3 doped with divalent calcium. This research was undertaken to study the effects of the dopant on the conductivity of the host.

Chapter 2 deals with the theory of dielectrics, relaxation phenomena and ionic conductivity. Chapter 3 introduces the LaF_3 structure while chapter 4 describes experimental procedures and apparatus. Results and data analysis are discussed in chapter 5 and finally, chapter 6 contains a summary and suggestions for further research.

Chapter 2

2-1 Dielectric Theory

A perfect dielectric is an insulator or a non-conductor of electricity. However, the dielectric exhibits the interesting ability to increase the amount of charge stored between two conducting plates at a constant electric potential or voltage. Studies of this phenomenon show that the response of dielectrics to an applied field is governed by two parameters. The first is ε', the real part of the dielectric constant, which describes the ability of the charges within the dielectric to polarize or align themselves with the applied field. The second parameter is ε'', the complex part of the dielectric constant, which is related to the energy dissipated during polarization.

The capacitance, C, of any system is given by the equation:

$$C = \frac{Q}{V} \qquad\qquad 2.1$$

where Q is the charge stored in the capacitor and V is the electric potential across the capacitor. If the capacitor under consideration is a perfect parallel plate capacitor (like that shown in figure 2-1a) the equation reduces to:

$$C = \frac{\varepsilon_0 A}{d} \qquad\qquad 2.2$$

9

where ε_0 is the permittivity of free space, A is the area of the plates and d is the distance seperating the plates.

Now, if a dielectric is placed in between the plates, a charge realignment occurs within the dielectric (see Figure 2-1b.) This realignment in turn tends to compensate for some of the charge on the plates. Thus, in order to maintain a constant potential across the capacitor, more charge must gather on the plates. If Q represents the charge on the capacitor before the insertion of the dielectric and Q' the charge after:

$$Q' = \varepsilon'Q \qquad \qquad 2.3$$

where ε' is the real part of the dielectric constant discussed earlier.

This in turn implies:

$$C' = \varepsilon'C \qquad \qquad 2.4$$

where C is the original capacitance of the system and C' is the enhanced capacitance after the addition of the dielectric.

As stated earlier, a dielectric both polarizes, or stores charge like a capacitor, and dissipates energy like a resistor. These facts lead to a simple electric model for the dielectric.
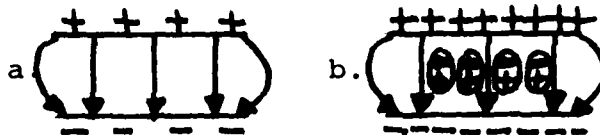
Figure 2-1
2-1a Shows a perfect parallel plate
capacitor. 2-1b Shows charge realignment
which occurs when a dielectric is placed
between the plates.
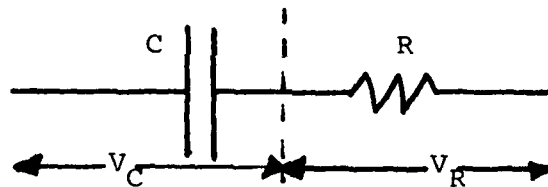
Figure 2-2
Figure 2-2 shows a simple model for a
dielectric. V_C represents the voltage across
the capacitor, while V_R represents the
voltage across the resistor. (V. V. Daniels
in Dielectric Relaxation, New York: Academic
Press, Inc., 1967, p. 2.)

11

This model consists of a capacitor of capacitance C in series with a resistor of resistance R.

Electrical theory demands that:

$$V = V_C + V_R \qquad \text{2.5}$$

where V is the voltage across the system and V_C and V_R have their previously defined meanings. If we assume that the applied voltage changes in time, then it is reasonable to futher assume that the charge on the capacitor given in equation 2.1 also changes in time. Thus:

$$\frac{dQ}{dt} = C\frac{dV}{dt} \qquad \text{2.6}$$

while by definition:

$$I = \frac{dQ}{dt} \qquad \text{2.7}$$

where I is the current through the dielectric. Since C and R are in series, it holds that I is also the current through the resistance, R. V_R is then given by the relation:

$$V_R = RI \qquad \text{2.8}$$

From equation 2.5 it follows that:

$$V = \frac{Q}{C} + R\frac{dQ}{dt} = V_c + V_R$$

or

$$CV = \tau\frac{dQ}{dt} + Q$$

12

$$CV = RC\frac{dQ}{dt} + Q \qquad . \qquad\qquad 2.9$$

The quantity, $\tau = RC$, is called the relaxation time and relates to the time delay of the response of the system to an applied field.

An applied sinusoid can be represented by the complex quantity

$$V^*(\omega, t) = V_0 e^{i\omega t} \qquad\qquad 2.10$$

where $V^*(\omega, t)$ is the instantaneous voltage at any time, t, V_0 is the amplitude and i is the $\sqrt{-1}$, ω is the applied angular frequency and e is the base for the natural logarithms. (NOTE: An asterisk will be used throughout this manuscript to represent a *complex quantity*.) This leads us to define the complex quantities $Q^*(\omega, t)$ and $C^*(\omega)$ where:

$$V^*(\omega, t) = \frac{Q^*(\omega, t)}{C^*(\omega)} \qquad\qquad 2.11$$

Combining equations 2.10 and 2.11 we obtain:

$$Q^*(\omega, t) = C^*(\omega) V_0 e^{i\omega t} \qquad\qquad 2.12$$

which in turn implies:

$$I^*(\omega, t) = \frac{dQ^*(\omega, t)}{dt} = i\omega C^*(\omega, t) V^*(\omega, t) \qquad\qquad 2.13$$

Plotting $I^*(\omega, t)$ and $V^*(\omega, t)$ at some instant, t_0:

13
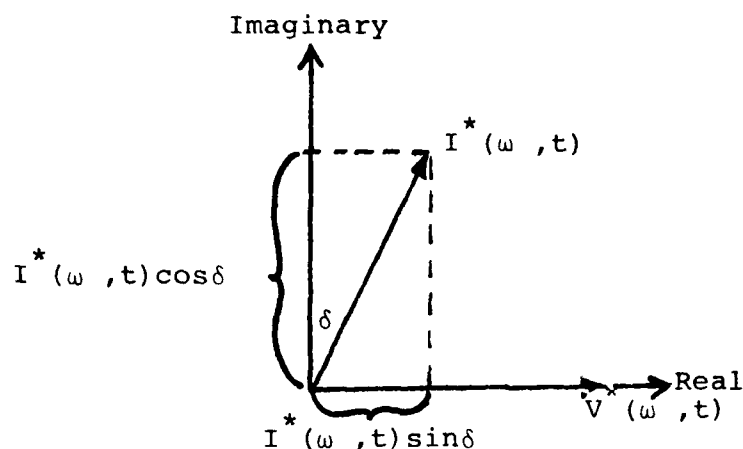
Figure 2-3

Figure 2-3 shows $I^*(\omega,t)$ and $V^*(\omega,t)$ at some instant.

If we define the following:

$$\varepsilon'' = \sin\delta$$
$$\varepsilon' = \cos\delta$$

2.14

Then the current in the imaginary direction is:

$$I = \varepsilon' I^*(\omega,t)$$

2.15

While the current in the real direction is given by:

$$I = \varepsilon'' I^*(\omega,t)$$

2.16

The imaginary current can be described as the current going toward the charging of the capacitor in the circuit in Figure 2-2. So, the quantity ε' is related to the polarization of the dielectric that the circuit represents. Similarly, the real current describes that current which is used to dissipate heat. Thus ε'' is related to the energy loss of the

14

dielectric.

Actually, the circuit which describes a true dielectric is more complex than the circuit discussed here. However, this analysis shows the origins of the real and complex parts of the dielectric constant.

Thus far, it has been said that dielectrics polarize with no mention of the method of that polarization. It has been found that charge realignment within the dielectric is due to many mechanisms, with three being predominant. The first is electronic realignment which comes about by reorientation of electrons about individual atoms within the dielectric. Second is ionic realignment which occurs by the displacement of atoms relative to each other within molecules of the dielectric. Finally, the third mechanism is dipolar realignment or relaxation in which molecules with permanent dipoles align with the applied field. At low frequencies, all three mechanisms contribute to the dielectric constant. However, as frequency increases, inertial considerations imply that the relatively heavy molecule will be unable to align quickly enough to significantly affect the dielectric constant. Thus, at intermediate frequencies, only ionic and electronic mechanisms are important. Similarly, at yet higher frequencies, the atoms involved in the ionic mechanism can no longer

15

align leaving only electronic realignment significant.
Figure 2-4 gives a graphical representation of the
change of the real part of the dielectric constant with
frequency.
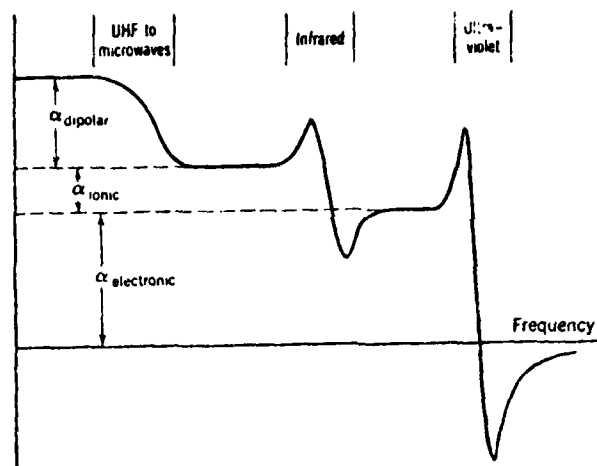
Figure 2-4

Figure 2-4 shows the frequency dependence of ϵ'
the real part of the dielectric constant.
(C. Kittel in Introduction to Solid State
Physics, New York: John Wiley and Sons, Inc.,
1976, p.411)

16

2-2 Relaxation Phenomena and Dielectric Relaxation

A relaxation is the delayed response of a system
to an applied stimulus. In the case of a dielectric,
it is the delayed charge realignment discussed in
section 2-1. In general, systems exhibiting relaxation
are governed by a differential equation of the type:

$$\tau \frac{dx}{dt} + x = y \qquad\qquad 2.17$$

where τ is the relaxation time, t is time and x and y
are arbitrary variables.

When working at low frequencies, it can be
assumed that electronic and ionic relaxation is
instantaneous. (See figure 2-4 section 2-1.) If ε_s is
the real part of the dielectric constant for a static
field and ε_∞ is the real part of the dielectric
constant at high frequency (here assumed to be the
electronic and ionic contributions), then the real part
of the dielectric constant due to diploes, ε_D, is
given by:

$$\varepsilon_D = \varepsilon_s - \varepsilon_\infty \qquad\qquad 2.18$$

The governing equation for dipolar relaxation becomes:

$$\frac{dP_D^*(t)}{dt} + P_D^*(t) = (\varepsilon_s - \varepsilon_\infty)t \qquad\qquad 2.19$$

where $P^*(t)$ is the dipolar polarization and all other
variables have their previously defined meanings.

17

Solution of this differential equation for a sinusoidal
V(t) leads to the complex solution:

$$P_D^*(t) = \frac{(\varepsilon_s - \varepsilon_\infty)V^*(\omega,t)}{1 + i\omega t} \qquad 2.20$$

The quantity $\varepsilon = \varepsilon'(\omega) - \varepsilon''(\omega)$ called the
total dielectric constant can be defined such that:

$$\varepsilon^*(\omega) - \varepsilon_\infty = \frac{P_D^*(t)}{V^*(\omega,t)} = \frac{\varepsilon_s - \varepsilon_\infty}{1 + i\omega\tau} \qquad 2.21$$

This in turn can be separated into its real and
imaginary parts such that:

$$\varepsilon'(\omega) = \varepsilon_\infty + \frac{\varepsilon_s - \varepsilon_\infty}{1 + \omega^2\tau^2} \qquad 2.22$$

$$\varepsilon''(\omega) = (\varepsilon_s - \varepsilon_\infty)\frac{\omega\tau}{1 + \omega^2\tau^2} \qquad 2.23$$

These equations are called the Debye Equations. A more
in-depth study of dipolar relaxation on a molecular
basis yields information about the quantity ε_s. A
molecular dipole can be modeled using the bistable
potential-well shown in figure 2-5.

18
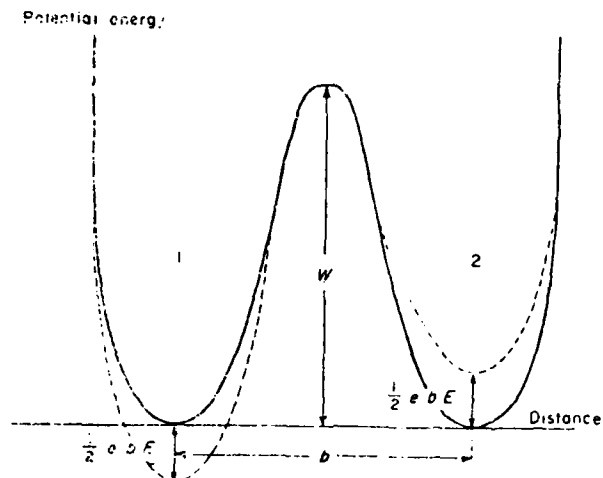
Figure 2-5

Figure 2-5 shows a bistable potential
well. The dotted lines represent the well
modified by an electric field. (V. V.
Daniels in Dielectric Relaxation, New York:
Academic Press, Inc., 1967, p. 21.)

Two charges of opposite sign constitute the dipole with
one charge sitting in the center while the other sits
in the bottom of one of the wells. The dipole may be
in either orientation. With no applied field, both
orientations are equally likely. However, when a field
is applied, the potential-well is modified as indicated
by the dashed lines in figure 2-5.

Assuming that equilibrium exists, the Maxwell-
Boltzmann distribution can be applied and it is found
that:

$$N = N_0 \exp(-E/kT) \tag{2.24}$$

where N_0 is the number of dipoles in a given state, N
is the number of dipoles with sufficient energy to make
a transition from that state to the other, E is the
height of the energy barrier between the states, T is
the absolute temperature and k is the Boltzmann
constant. Since E_2 (the energy barrier going from
state 2 to state 1) is smaller than E_1 (the energy
going from state 1 to state 2) transitions to state 1
are enhanced.

It is reasonable to assume that the actual
frequency of transition is proportional to the number
of dipoles with sufficient energy to make a transition.
Thus:

$$f \propto N$$
$$f \propto N \exp(-E/kT)$$

$$f = f_0 \exp(-E/kT) \qquad\qquad 2.25$$

Also it can be shown that the relaxation time, τ , is given by:

$$\tau = \frac{1}{2f} = \tau_0 \exp(E/kT) \qquad\qquad 2.26$$

τ_0 is known as the reciprocal frequency factor. Finally, further application of the Boltzmann distribution between the preferred and non-preferred sites gives:

$$\varepsilon_s - \varepsilon_\infty = \frac{N_0 P^2}{3\varepsilon_0 kT} = \alpha_D \qquad\qquad 2.27$$

where P is the dipole moment and all other variables have their same meanings.

α_D is known as the dipolar polarizability and is further defined by combining all other variables over T so that:

$$\varepsilon_s - \varepsilon_\infty = \alpha_D = \frac{A}{T} \qquad\qquad 2.28$$

where A is now known as the dipole strength.

The Debye equations may now be written:

$$\varepsilon' = \varepsilon_\infty + \frac{A}{T(1 + \omega^2\tau^2)} \qquad\qquad 2.29$$

$$\varepsilon'' = \frac{A\omega\tau}{T(1+\omega^2\tau^2)} \qquad\qquad 2.30$$

Another quantity used in the study of

21

dielectrics and conductors is the conductivity, σ.
Conductivity is related to the power loss which occurs
during reorientation. Since power is energy per unit
time, it is logical that:

$$\sigma \propto \omega \varepsilon''$$

since ω is in the units of $\sec^{-1}$ and ε'' is related
to energy loss during relaxation. In fact:

$$\sigma = \varepsilon_0 \omega \varepsilon'' \qquad \qquad 2.31$$

where ε_0 is the permittivity of free space. Combining
equations 2.30 and 2.31:

$$\sigma_{dipolar} = \frac{\varepsilon_0 \omega^2 A \tau}{T(1 + \omega^2 \tau^2)} \qquad \qquad 2.32$$

Equation 2.32 and the defining equation for relaxation
time, equation 2.26, make-up the governing equations
for dipolar conductivity.

2-3   Ionic Conductivity

Ideal ionic solids can be considered a regular array of positive and negative charges. However, no ionic crystal is truely ideal. Real crystals exhibit faults or defects in their array. These defects are of two general types, vacancies and interstitials.

A vacancy is the absence of an entire ion. It can be caused by two major phenomena. The first is called the " Schottky defect." This mechanism proposes the existence of equal numbers of positive and negative vacancies which insures ultimate charge neutrality. This type of defect is intrinsic and occurs even in the "perfect" crystal. The second major source of vacancies is impurity ions. If an impurity ion of a different valence replaces an ion in the crystal, vacancies must occur in order to maintain charge neutrality.
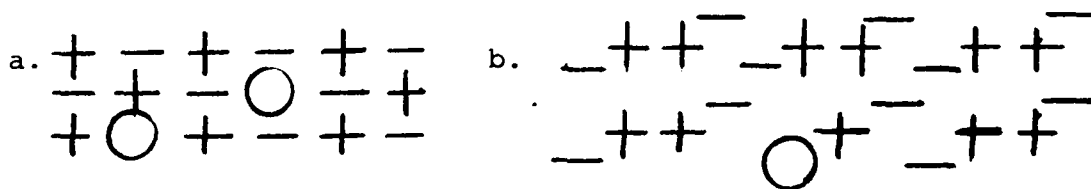
Figure 2-6
(a) Shows Schottky Defects. (b) Shows a more complicated ionic crystal in which a 1+ replacing a 2+ causes a vacancy.

23

An interstitial ion is an ion which resides in a
site between the normal sites of the ionic array.
Again, intertitials can be caused by two major
mechanisms. The first, the "Frenkel defect," is
similar to the Schottky defect discussed earlier in
that it is intrinsic. In the Frenkel defect, an ion
absents its normal array site and occupies an
interstitial site. Second, impurity ions may also
cause interstitials in order to charge compensate.

Figure 2-7
(a) Shows a Frenkel defect. (b) Shows an
interstitial caused by a 2+ replacing a 1+ in
the lattice.

Defects like those described above allow ions to
move within the ionic crystal. Mobile ions allow
charge to be conducted through the solid. Each type of
defect has associated with it some energy of formation
and some energy of motion which combine to form an
activation enthalpy, E_A, for motion of the defect.
(NOTE: The terms energy and enthalpy will be used
interchangably in this work.) As charge is conducted
through the solid, energy is dissipated. Ionic

conductivity, σ , is related to the power loss during this phenomenon. Ionic conductivity is given by the Arrhenius equation:

$$\sigma_{ionic} = \frac{\sigma_0}{T} \exp(-E_A/kT)$$
2.33

where σ_0 is a pre-exponential factor, T is the absolute temperature and E_A is the activation energy for the mechanism in question.

It can be seen from equation 2.34 that a plot of log(σ T) versus 1/T will yield a straight line which has a slope simply related to the activation enthalpy. Such a plot for a true ionic solid has several regions of differing slope. (See figure 2-8.) Region I is termed the "intrinsic region." The dominant defects in this region are intrinsic Schottky and Frenkel defects. Region II is known as the "extrinsic region." In this region, the dominant defects are those created by impurity ions. Region III, the "association region," relates to the situation in which defect association is the major defect. An example of defect association is the creation of a bound vacancy and impurity ion pair. In this region, the activation energy is a combination of both the energy of association and the energy of motion. Specifically:

$$E_A = \frac{E_a}{2} + E_m$$
2.34

25

At temperatures lower than those shown in figure 2-8, other mechanisms, such as dipolar dielectric relaxtion, may contribute to the conductivity.
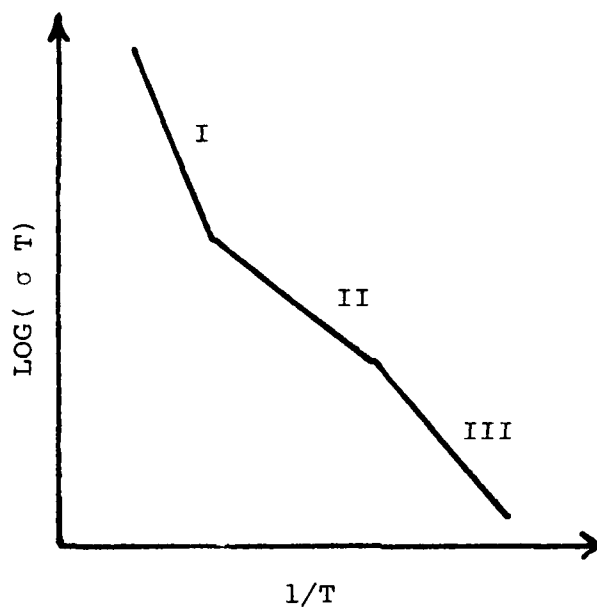
Figure 2-8
Figure 2-8 shows a typical conductivity plot
for an ionic solid.

Chapter 3

3-1   The Structure of LaF_3

The structure of LaF_3 has been the subject of several studies. In 1931, Oftedal proposed a point group of $P6_3/mcm$ with hexagonal symmetry [7]. However, more recent research has indicated that the structure has a closely related trigonal structure with cell parameters of $a=b=7.185 \overset{0}{A}$ and $c=7.351 \overset{0}{A}$ [8].

Figure 3-1 shows a schematic of the structure of LaF_3 as proposed by the latter work above. Notice that the lanthanum ion, located at the center, is nine-fold coordinated. That is, it has nine nearest neighbor fluorine ions at about equal distance. Each fluorine ion site has been numbered for ease of reference. There are four pairs of equidistant fluorine ions. These are: pair 5-6 at $2.42 \overset{0}{A}$, pair 1-7 at $2.46 \overset{0}{A}$, pair 2-9 at $2.49 \overset{0}{A}$, and pair 4-8 at $2.64 \overset{0}{A}$. Fluorine ion site 3 is unpaired at $2.44 \overset{0}{A}$. These pairs have significant meaning in a model for relaxation proposed in Chapter 5. Table 3-1 gives the coordinates of all the sites relative to the lanthanum ion site assumed to be at (0,0,0).

Table 3-1

SITE	X	Y	Z
1	0.065	0.174	2.433
2	2.325	0.143	1.242
3	1.222	2.116	0.000
4	-1.214	-2.165	1.242
5	1.222	-2.033	0.463
6	-2.371	0.042	0.463
7	0.119	0.143	-2.433
8	-1.268	-2.134	-1.243
9	-1.039	2.085	-1.243

NOTE: All coordinates are in units of Å.
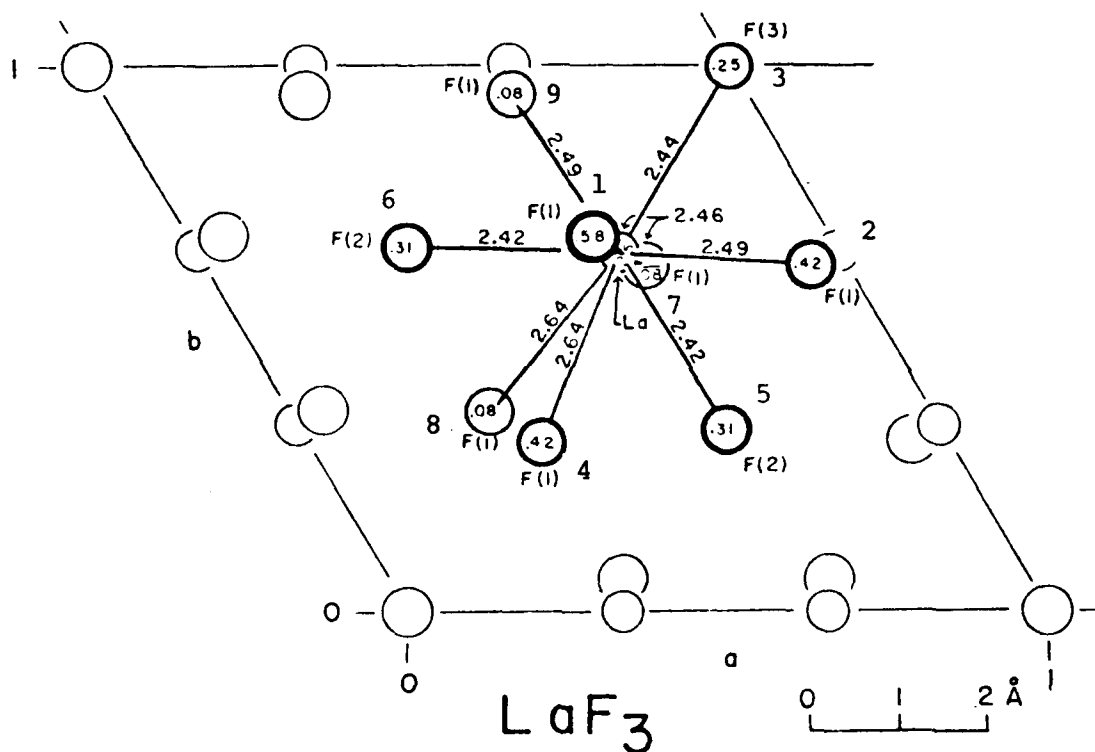
LaF₃

Figure 3-1
Figure 3-1 shows the structure of LaF₃. (A. Zalkin,D. H. Templeton, and T. E. Hopkins [8].)

28

Chapter 4

4-1   Experimental Procedure

Crystals used in this research were obtained from Optovac,Inc. The dopant, calcium, was introduced in concentrations from 0.01% to 1.0% and the samples were cut such that two orientations , parallel and perpendicualar to the c-axis, were available for experimentation. Those crystals oriented parallel to the c-axis were about 10mm x 10mm x 2mm, while the other samples were round and about 8mm in diameter. The crystals were ground to a final thickness of about 1mm.

Next, aluminum electrodes were evaporated onto the crystals. The crystals were cleaned with freon and then placed in a bell jar which was evacuated to a pressure of about 10^{-4} torr. Argon gas was then bled into the bell jar and a high-voltage discharge was used to clean the sample surfaces. This was done to insure a tight bond between the crystals and the electrodes.

Samples which were large enough were evaporated in the standard three terminal configuration. (See figure 4-1a.) This configuration minimizes fringe effects. The insulating gap shown in figure 4-1a was obtained by placing a guard ring on the sample during the electrode evaporation. Those samples too small for the three terminal configuration were fitted with

insulating rings, again in an attempt to minimize

fringe effects.   (See figure 4-lb.)
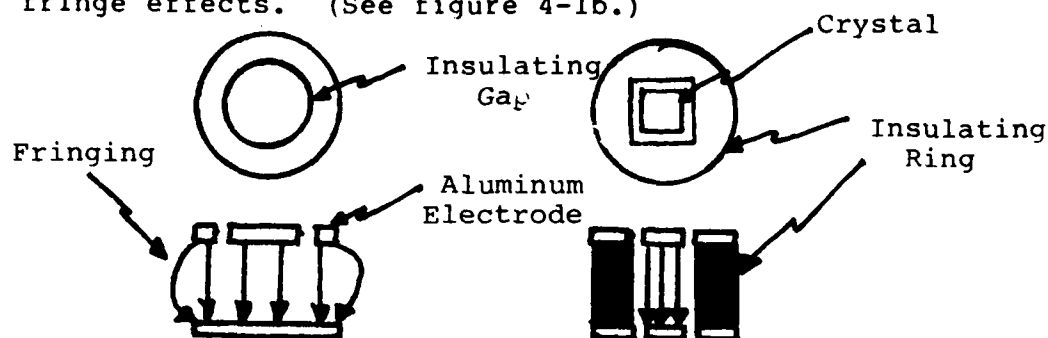
Figure 4-1
(a) Shows the three terminal configuration.
Measurements were taken inside the insulating
gap. (b) Shows an insulating ring. The
permittivity of the ring helped to reduce
fringing.

Capacitance and conductance divided by angular

frequency (G/ω) measurements were then made utilizing

a specially modified, fully-automatic, microprocessor

controlled General Radio transformer ratio arm bridge.

A basic schematic of the bridge is shown in figure 4-2.

After balancing the bridge, the unit automatically

prepared a hard copy of the data on a computer terminal

and cut a paper tape of the data for input into the

computer at a later time. Some 20,000 data points were

taken in this manner.

The samples were maintained at constant

temperature in a Cryogenics Associates cryostat.

Through the temperature range 80-310 K, cooling was

done with liquid nitrogen, while at lower temperatures,

5.4-80 K, liquid helium was used. Temperature was

controlled by the use of a Wheatstone's Bridge with a

germanium (5.4-30 K) or a platinum (30-310 K)

resistance thermometer. Feedback (integral,

proportional and differential) was used in order to

maintain temperature to within .01 K of the desired

temperature.

Figure 4-2

Figure 4-2 shows a schematic of the bridge.
The the bridge works by balancing the in-
phase and out-of-phase voltage by positioning
the tap (a) until the detector reads zero.
The in-phase voltage is proportional to G/ω
and the out-of-phase voltage is proportional
to C.
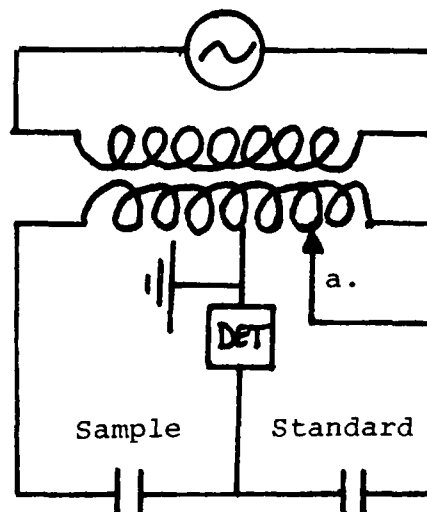
31

4-2 Determination of ϵ'' and σ

Equations 2.2 and 2.4 relate capacitance to area thickness, and the real part of the dielectric constant. Changes in thickness and area are in turn related to the coefficient of thermal expansion. Thus, changes in the real part of the dielectric constant are tied to changes in capacitance and to the coefficient of thermal expansion. In fact:

$$\epsilon'(T) = \epsilon_{300} \frac{C(T)}{C_{300}} \exp\left(-\int_T^{300} \alpha_p dT\right) \qquad 4.1$$

where $\epsilon'(T)$ is the real part of the dielectric constant at some temperature, T, C(T) is the capacitance of the sample at the same temperature, ϵ'_{300} and C_{300} are the values of the real part of the dielectric and the capacitance at 300 K ,respectively, and α_p is the isobaric coefficient of linear thermal expansion for LaF_3. A computer program was used to integrate the exponent in 10 K increments.

ϵ'_{300} was determined for each sample using standard geometrical techniques assuming each sample to be a perfect parallel plate capacitor and applying equations 2.2 and 2.4 to the capacitance measured at 300 K. The weight of the electrodes was negligible. Knowing the density, ρ , of LaF_3 and the thickness, area was easily abtained from the mass using the following relationship:

32

$$A = \frac{V}{d} = \frac{m}{\rho d} \qquad\qquad 4.2$$

where A is the area of the sample, V the volume and m
the mass. Area was also determined through direct
measurement using a scanning microscope. Good
agreement was obtained between the two methods. Table
4-1 shows the values of A, d, and ε'_{300} measured.

<div align="center">Table 4-1</div>

ORIENTATION	CONC.	THICKNESS (cm)	AREA[1] (cm)	AREA[2] (cm)	ε_{300}
to c-axis	0.01%	.125	.8881	.8924	78.8
	0.1 %	.116	.8883	.8438	103.2
	0.3 %	.126	.8684	.8803	85.3
to c-axis	0.01%	.107	=====[3]	.6207	699.7
	0.03%	.100	.8099	.8185	530.3
	0.1 %	.098	.8484	.8660	605.9
	0.3 %	.107	=====[3]	.6207	459.4

NOTE: 1) Area determined from equation 4.2 using ρ =5.936 gm/cm
        2) Area determined using scanning microscope.
        3) These crystals were evaporated using the three terminal
           configuration. The area inside the insulating gap was
           known.

It can be shown that:

$$\varepsilon'' = \frac{Gd}{\varepsilon_0 \omega A} \qquad\qquad 4.3$$

where all variables have their previously stated
meanings. Rearranging we obtain:

$$\varepsilon'' = \frac{G}{\omega}\left(\frac{d}{\varepsilon_0 A \varepsilon'}\right)\varepsilon' \qquad \qquad 4.4$$

The second term is merely the capacitance of the system, so:

$$\varepsilon'' = \frac{\varepsilon' G}{\omega C} \qquad \qquad 4.5$$

Finally, combining equations 2.31 and 4.5, we obtain:

$$\sigma = \frac{\varepsilon_0 \varepsilon' G}{C} \qquad \qquad 4.6$$

Chapter 5

5-1   Results

In conductivity studies, it is customary to
present data in the form of LOG(σ T)-vs-S/T where S is
some convenient scaling factor. In this work, S=1000.

Typical results of measurements taken
perpendicular to the c-axis appear in figure 5-1. The
graph shows a thermally activated association region
(A) followed by a large dielectric relaxation
exhibiting dipolar characteristics (B). Finally, the
graph shows two smaller dielectric relaxations at lower
temperatures (C). Figure 5-2 shows typical results for
measurements taken parallel to the c-axis. Again, a
thermally activated region (A') followed by a dipolar
dielectric relaxation (B') is observed. However, three
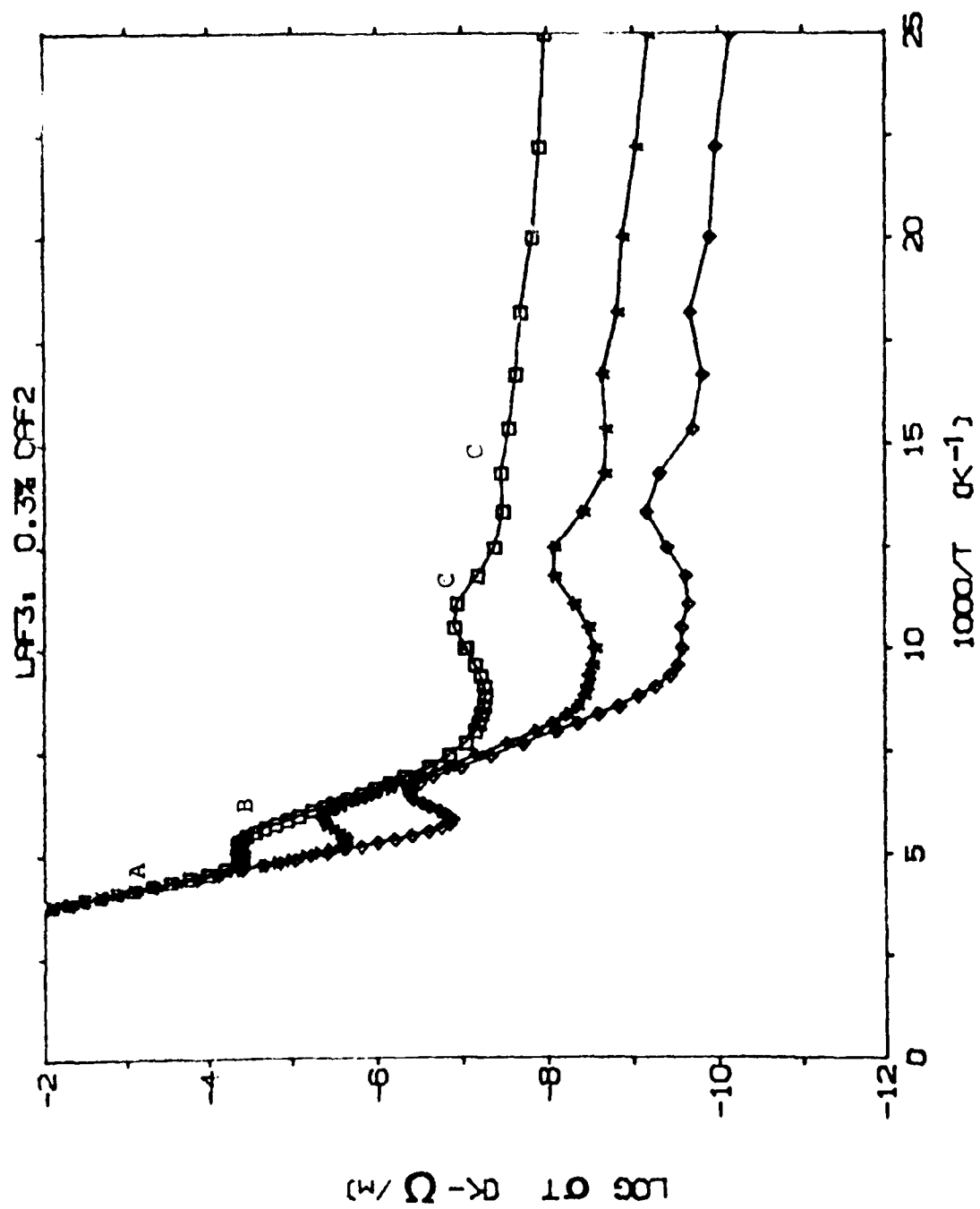smaller relaxations (C') are present in this data.

Figure 5-1

36

LaF3, 0.3% CaF2

Figure 5-2

37
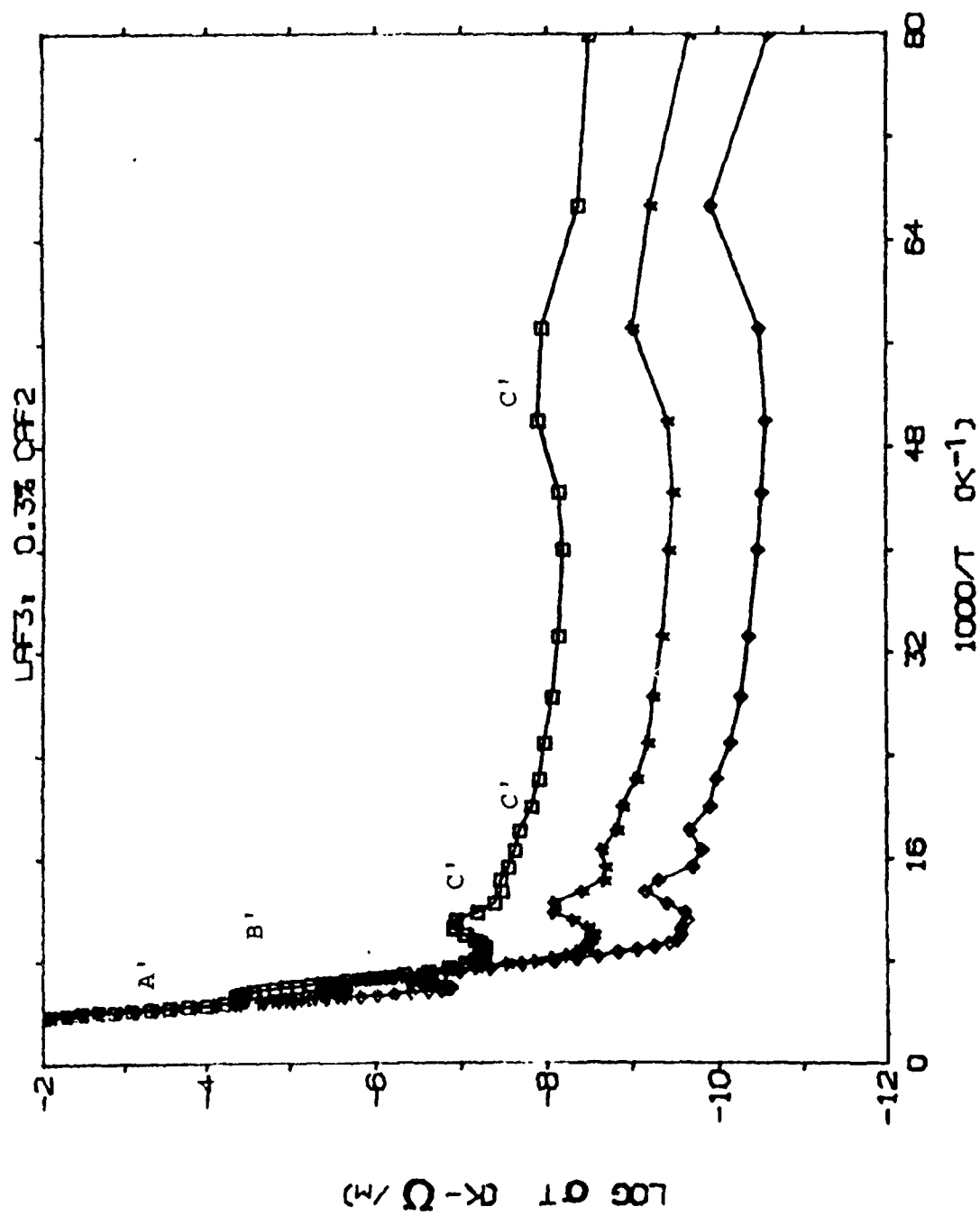
5-2 Data Analysis

Data in the dipolar region was analyzed using a computer fitting routine. In this analysis it was assumed that the total conductivity, σ , could be modeled as the sum of the conductivity due to ionic conductivity and that due to dipolar conductivity; so that:

$$\sigma = \sigma_{ionic} + \sigma_{dipolar} \qquad 5.1$$

σ_{ionic} was determined using equation 2.33 and $\sigma_{dipolar}$ was determined using a modified version of equation 2.32.

As mentioned earlier, the quantity of interest in this study was LOG(σ T). Therefore, this was the quantity which was fit by the computer program used. The equations used in the fitting routine were:

$$\sigma_{ionic}T = \sigma_0 \exp(-E'/kT) \qquad 5.2$$

$$\sigma_{dipolar}T = \frac{A\omega\cos(\frac{\alpha\pi}{2})}{2\{\cosh(1-\alpha)x + \sin(\frac{\alpha\pi}{2})\}} \qquad 5.3$$

$$x = \ln\omega\tau$$

$$A = (\epsilon_s - \epsilon_\infty)\epsilon_0$$

$$\tau = \dot{\tau}_0 \exp(E/kT) \qquad 5.4$$

$$\sigma T = \sigma_{ionic} T + \sigma_{dipolar} T \qquad \text{'} \qquad\qquad 5.5$$

These equations led to the following six adjustable
parameters: E', E, $\ln\tau_0$, $\ln\sigma_0$, A, and α . E' is the
activation enthalpy in the association region, while E
is the activation enthalpy in the dipolar region. $\ln\tau_0$
and $\ln\sigma_0$ are the natural logs of the reciprocal
frequency factor and pre-exponential, respectively.
Best fit parameters for measurements taken
perpendicular to the c-axis are shown in table 5-1 and
a typical best fit curve for the same data is found in
figure 5-3. Similarly, table 5-2 gives the best fit
parameters for the data taken parallel to the c-axis
and figure 5-4 shows a plot of these parameters for one
of the samples.

LaF$_3$:Ca Perpendicular to the C-Axis

Concentration		Association Region		Dipolar Contribution			α	RMS Dev
		E'(eV)	lnσ_0(K-℧/m)	E(eV)	$\tau_0(10^{-14}s)$	A(K)		
0.01%	1	0.506	16.4	0.335	1.61	29.1	0.10	0.023
	2	0.506	16.3	0.335	1.57	30.5	0.09	0.026
0.1%		0.488	15.9	0.312	9.16	218.5	0.13	0.024
0.3%		0.537	17.7	0.311	9.90	266.8	0.09	0.017

Table 5-1

LaF$_3$: 0.3% CaF$_2$

Best-Fit Curves
Perpendicular to c-axis

1000/T (K^{-1})

LOG σT (K-℧/m)

Figure 5-3

41
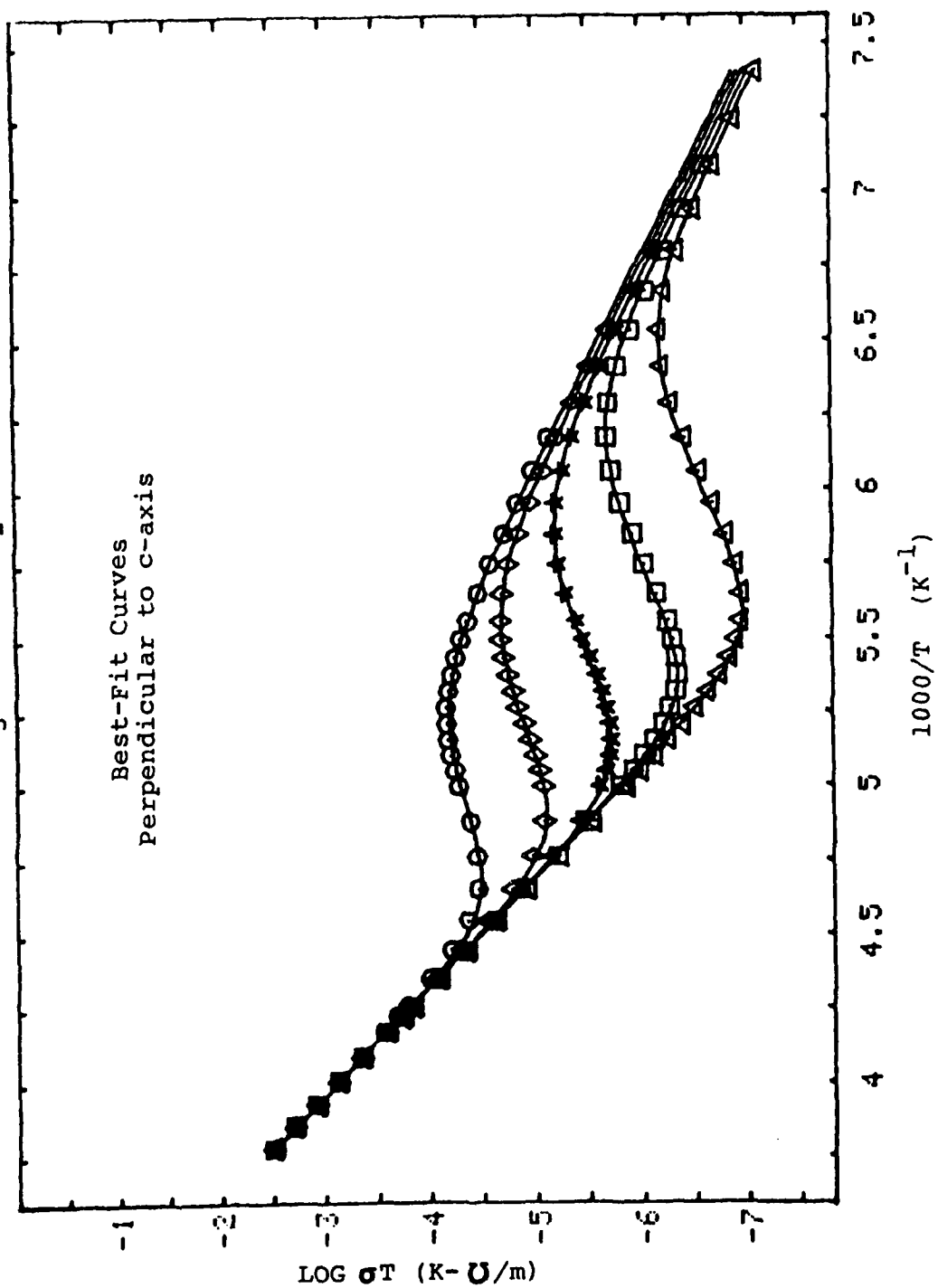
LaF_3:Ca Parallel to the c-Axis

Concentration	Association Region		Dipolar Contribution			σ	RMS Dev
	E'(eV)	$\ln \sigma_0$(K-℧/m)	E(eV)	τ_0(10^{-14}s)	A(K)		
0.01%	0.457	15.6	0.310	9.29	14.8	0.06	0.011
0.03%	0.457	15.4	0.302	16.1	20.0	0.05	0.014
0.1%	0.462	15.8	0.309	11.6	121.6	0.10	0.028
0.3%	0.512	17.6	0.309	11.6	174.3	0.07	0.020

Table 5-2

LaF$_3$: 0.3% CaF2

Best-Fit Curves
Parallel to c-axis

LOG σT (K- $\mho$/m)

1000/T (K^{-1})

Figure 5-4

43

5-3   Discussion

Figures 5-5 and 5-6 each show a schematic of ϵ''-vs-T. The former shows data taken perpendiculr to the c-axis and the latter shows data taken parallel to the c-axis. It can be seen that the two smalle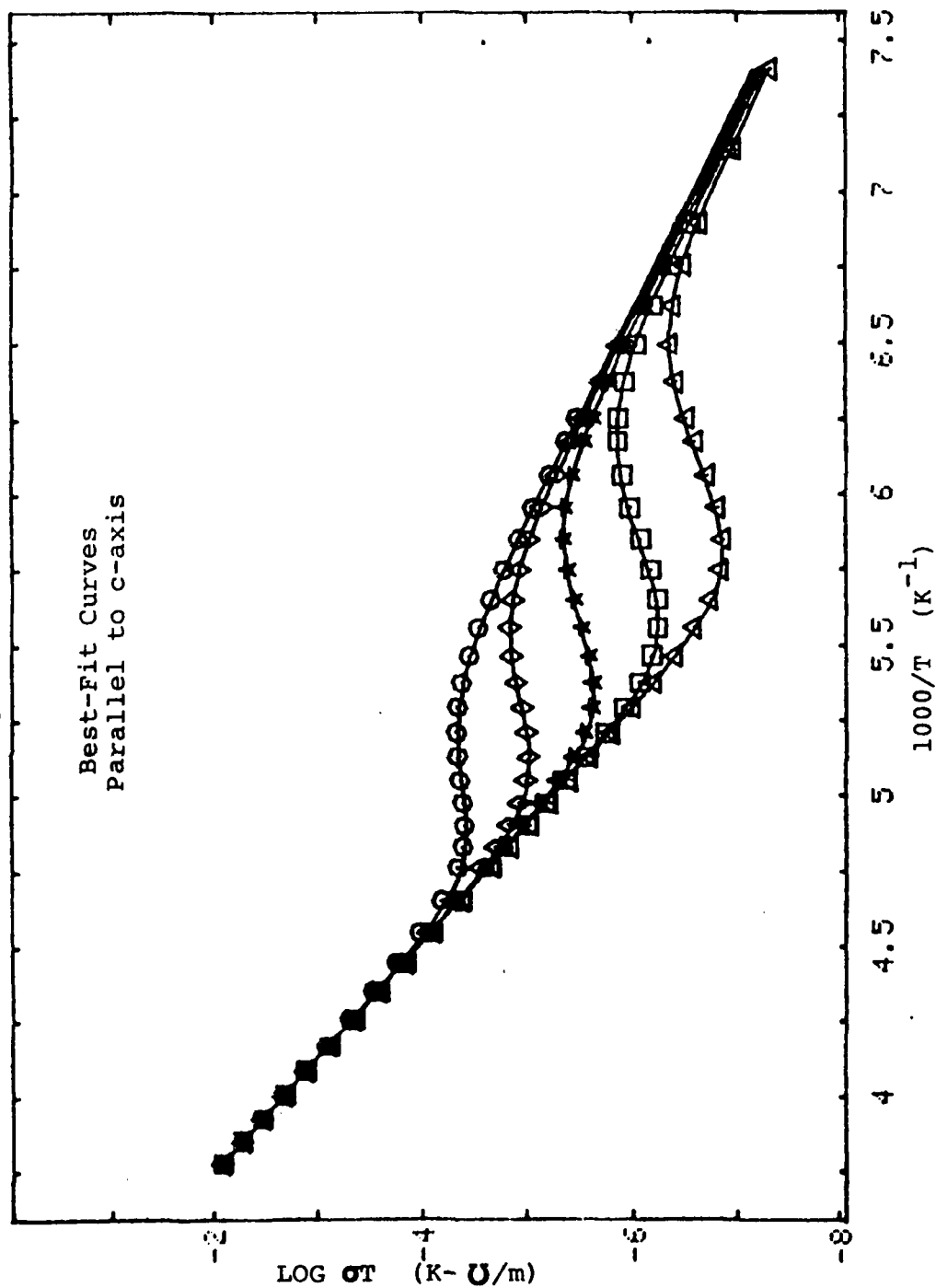r relaxations in the case of figure 5-5 and the three smaller peaks in the case of figure 5-6 are approximately two orders of magnitude smaller than the large dipolar relaxation which occurs in both sets of data. Analysis has shown that these relaxations are a function of neither concentration nor direction of applied field. For these reasons, these relaxations have been assigned as the results of trace impurities. However, further research into the low temperature region has been planned in order to verify this conclusion.

The principal doplar relaxation observed in this data has been attributed to a bound charge compensating fluorine ion vacancy relaxing about a substitutional alkaline earth ion. When Ca^{2+} replaces La^{3+} in the crystal lattice, a fluorine ion vacancy must bc created in order to insure charge neutrality. The undisturbed lattice contains a regular array of positive and negative charges. Thus, any removal of a negative charge makes the lattice relatively positive at that point and vice versa.
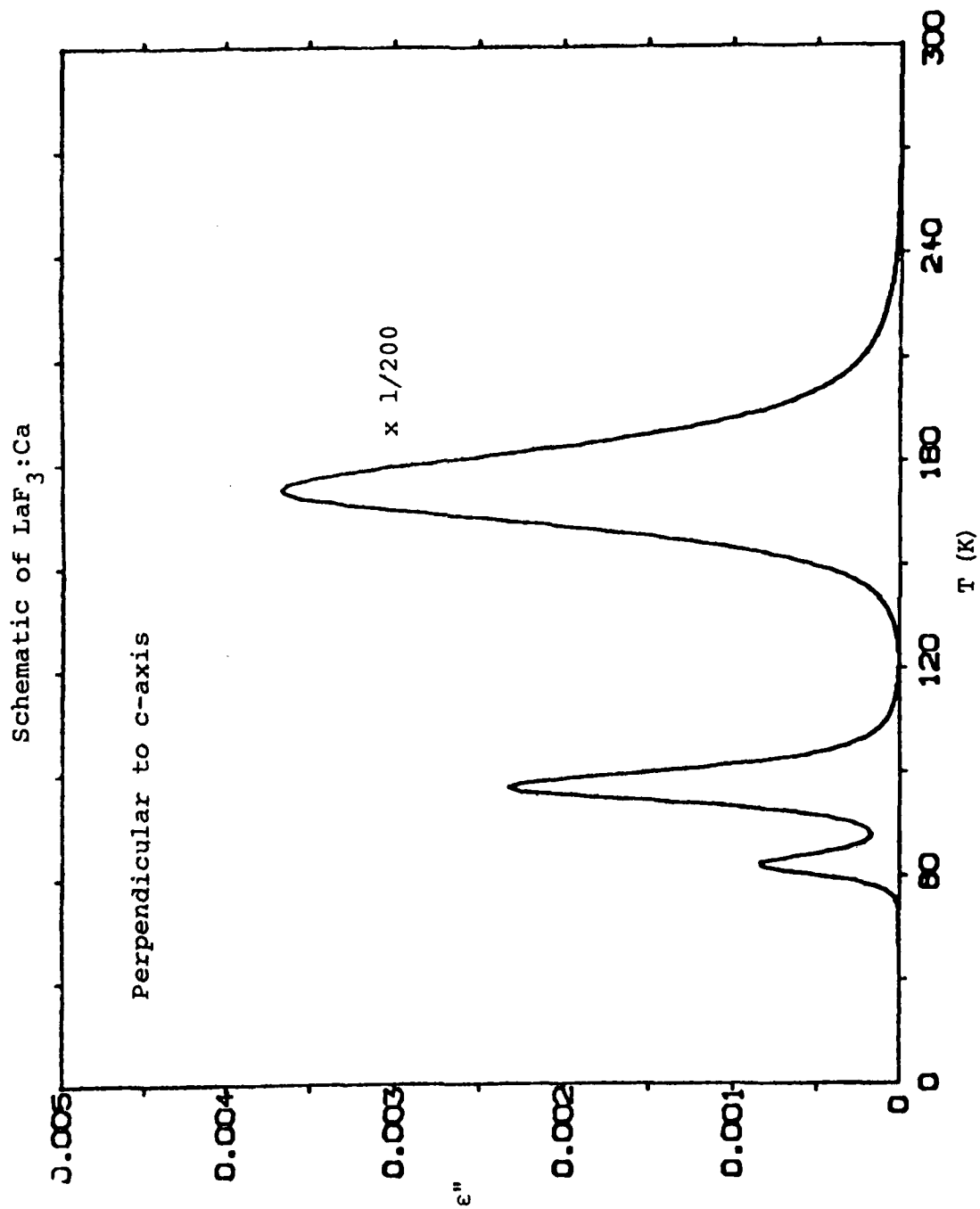
44

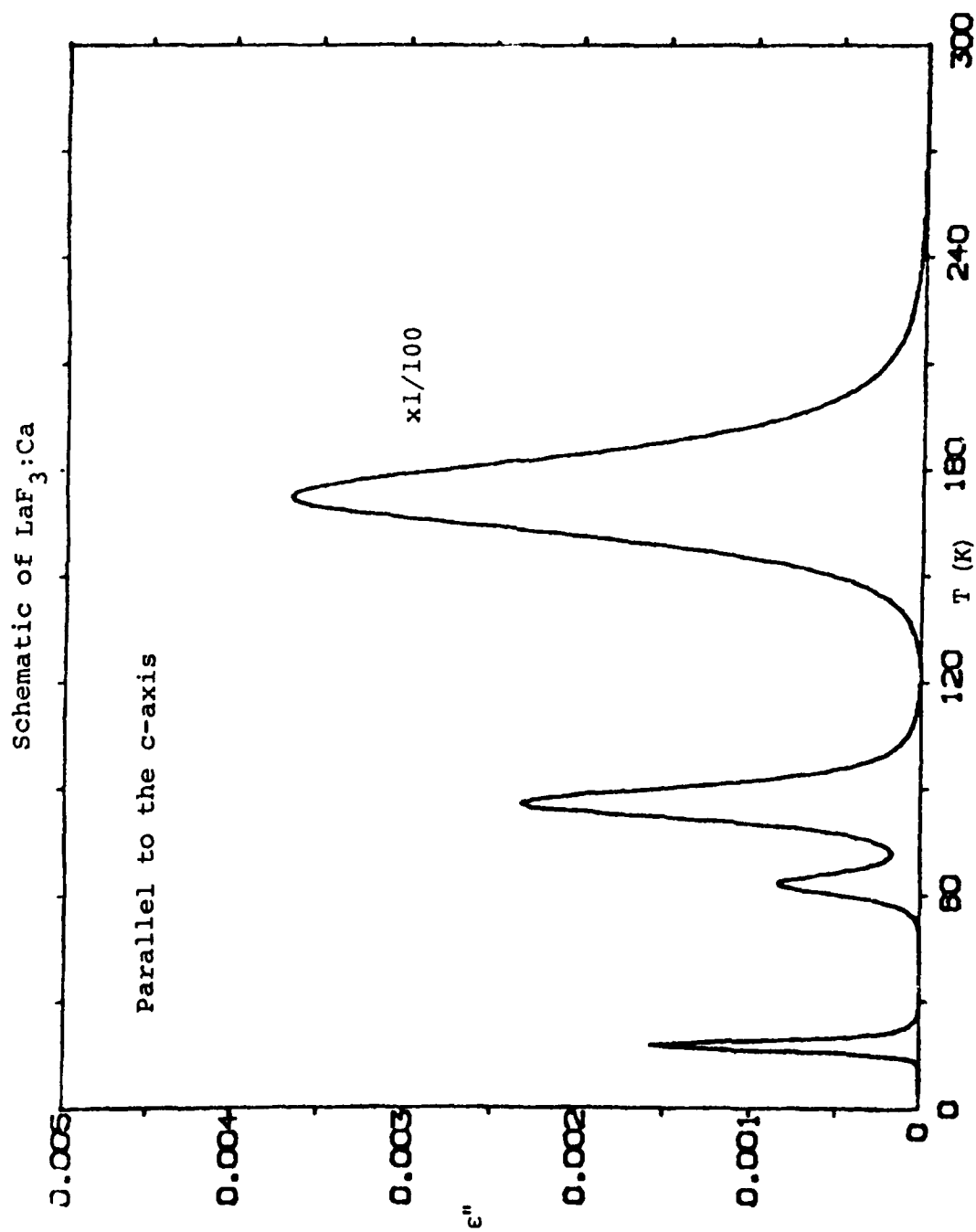Schematic of LaF$_3$:Ca

Perpendicular to c-axis

x 1/200

Figure 5-5

45

Schematic of LaF_3:Ca

Parallel to the c-axis

x1/100

ε''

0.005 0.004 0.003 0.002 0.001 0

T (K)

0 80 120 180 240 300

Figure 5-6

46

Therefore, the fluorine ion vacancy appears positive to the lattice, and the Ca^{2+} appears negative. A positive and neaqtive charge separated by a finite distance has thus been created. It is this dipole that is responsible for the large dielectric relaxation observed in the data.

As discussed in chapter 3, the lanthanum ion site in the crystal is nine-fold coordinated. The fluorine ion vacancy can be located in any of the nine fluorine ion sites. It is also able to move from site to site and it is this freedom which allows relaxation. Using the fluorine ion site positions given in chapter 3, inter-site distances can be determined. Table 5-3 shows the distance from one site to any other site. Notice the distances which have been underlined. All values are about 2.6 Å. There are no other distances between this value and approximately 3.0 Å.

Table 5-3

SITE	1	2	3	4	5	6	7	8	9
1	====	2.55	3.32	2.92	3.18	3.14	4.81	4.54	4.29
2	2.55	====	2.58	4.22	2.56	4.76	4.29	4.93	4.61
3	3.32	2.58	====	5.08	4.17	4.17	3.32	5.07	2.58
4	2.92	4.22	5.08	====	2.56	2.61	4.54	2.49	4.92
5	3.18	2.56	4.17	2.56	====	4.15	3.78	3.02	5.00
6	3.14	4.76	4.17	2.61	4.15	====	3.82	2.98	2.98
7	4.81	4.29	3.32	4.54	3.78	3.82	====	2.92	2.55
8	4.54	4.93	5.07	2.49	3.02	2.98	2.92	====	4.22
9	4.29	4.61	2.58	4.92	5.00	2.98	2.55	4.22	====

The model used to explain the dipolar relaxation proposes that vacancies can be transfered only between those sites which are separated by a distance of about 2.6 A. For example, a vacancy located in site 2 could be transfered to sites 1, 3 or 5 and no others. The model further proposes that relaxation occurs only between sites equidistant from the Ca^{2+} ion. That is to say, a fluorine ion vacancy could relax between sites 2 and 9, but it would pass through site 3 enroute. Table 5-4 shows the possible relaxations and their possible routes. The vacancy may pass in either direction during relaxation.

Table 5-4

PAIR	ROUTE
1-7	1-2-3-9-7
2-9	2-3-9
4-8	4-8
5-6	5-4-6

Tables 5-1 and 5-2 report an activation enthalpy in the dipolar region of $.31\pm.03$ eV for both directions of applied field. This energy represents the potential barrier over which the fluorine ion vacancy must pass during relaxation. In the bistable model of the dipole discussed in chapter 2, the activation enthalpy is the

barrier height between the wells. It has been found
empirically that, in general, the activation energy for
a bound vacancy is on the same order or slightly
smaller than that for mobile vacancy [9]. Chadwick [1]
reports a value of .28$\pm$.05 for the activation energy of
mobile fluorine ion vacancies in LaF_3. Consequently,
Chadwick's work supports the conclusion that the dipole
observed in the data is due to a bound fluorine ion
vacancy since the activation energy is close to that
for the motion of a free vacancy.

In section 2-3, it was said that the activation
energy in association region, E_A, was related to both
the energy of association, E_a, and to the energy of
migration, E_m. In fact, equation 2.35 states:

$$E_A = \frac{E_a}{2} + E_m$$

E_A is reported to be .49$\pm$.03 eV. Using the activation
energy in the dipole region as an approximate energy of
motion, an association energy of .38$\pm$.03 eV is
obtained.

Finally, comparing values of dipole strength for
samples of equal concentration:

$$A_\perp \cong 1.8 \; A_{\parallel}$$

where $A_\perp$ is the dipole strength perpendicular to the c-
axis and $A_{\parallel}$ is the dipole strength parallel to the c-
axis. This implies:

$$P_\perp^2 \cong 3.6\, P_\parallel^2$$

where $P_\perp$ is the perpendicular dipole moment, and $P_\parallel$ is the parallel dipole moment.

This result has yet to be rigorously explained. However, qualitatively, it is consistent with the present model. For a defect with activation enthalpies similar both both parallel and perpendicular to the c-axis [10]:

$$\frac{A_\perp}{A_\parallel} = \frac{P_\perp^2}{2P_\parallel^2}$$

Experimentally:

$$\frac{A_\perp}{A_\parallel} \cong 1.8$$

or:

$$\frac{P_\perp^2}{P_\parallel^2} \cong 3.6$$

If we sum the dipole moments of the relaxation pairs and resolve them into their parallel and perpendicular components:

$$\frac{P_\perp^2}{P_\parallel^2} \Big|_{theo} = \frac{P_{\perp\,1-7}^2 + P_{\perp\,2-9}^2 + P_{\perp\,4-8}^2 + P_{\perp\,5-6}^2}{P_{\parallel\,1-7}^2 + P_{\parallel\,2-9}^2 + P_{\parallel\,4-8}^2 + P_{\parallel\,5-6}^2} = 0.9$$

However, if we eliminate pair 1-7 because of its circuitous and unlikely route, we obtain:

$$\frac{P_\perp^2}{P_\parallel^2} \Big|_{theo} = 3.5$$

Although this calculation agrees well with the observed data, it must be refined to include such significant factors as differences in site population and energy.

Chapter 6

Summary

In summary, this research dealt with conductivity measurements of samples of LaF_3 doped in varying concentrations with Ca. The measurements showed a thermally activated region, $E_a = .38 \pm .03$ eV, a dipolar dielectric relaxation, $E = .31 \pm .03$ eV, and several smaller relaxations. The dipole relaxation is attributed to the reorientation of a bound fluorine ion vacancy about a substitutional Ca^{2+} ion. Evidence in favor of this identification is that the energy of motion of free vacancies reported by Chadwick [1] is close to that of bound vacancies reported in this work. Also, a difference in dipole strengths perpendicular and parallel to the c-axis has been explained qualitatively through the use of the model of the dipole. (The latter, however, needs further amplification.) The significance of these results is that the dipolar complex can be used to simulate free vacancies which are very difficult to study. In fact, pressure studies of LaF_3 which are planned will use this result. Other possible areas of future research include studying the effects of dopant ion size on the observed dipolar relaxation and studying the effects of interstitials caused by a tetravalent (4+) dopant. Work is also needed in theoretical modelling.

REFERENCES CITED

1. A. V. Chadwick, D. S. Hope, G. Jaroskiewicz and J. H. Strange, in Fast Ion Transport in Solids, edited by Vashishta, Mundy and Shenoy (Elsevier North Holland, Inc., 1979).

2. A. Sher, R. Solomon, K. Lee and M. W. Muller, Phys. Rev. 2, 144 (1966).

3. C. O. Tiller, A. C. Lilly and B. C. LaRoy, Phys.Rev. B 8, 10(1973).

4. R. Solomon, A. Sher and M. W. Muller, J. App. Phys. 37, 9 (1966).

5. P. H. Klein and W. J. Croft, J. App. Phys. 38, 4 (1967).

6. J. Schoonman, G. Oversluizen and K. E. D. Wapenaar, to be published in J. Solid State Ionics.

7. I. Oftedal, Z. Physik. Chem. B13, 190 (1931).

8. A. Zalkin, D. H. Templeton and T. E. Hopkins, Inorg. Chem. 5, 1466 (1966).

9. J. J. Fontanella, A. V. Chadwick, V. M. Carr, M. C. Wintersgill and C. G. Andeen to be published in J. Phys. C: Solid State Phys.

10. A. S. Nowick, Adv. Phys. 14, 101 (1965).

BIBLIOGRAPHY

Daniels, Vera V. Dielectric Relaxation. New York:
    Academic Press, Inc., 1967.

Hayes, W. "Superionic Conductors." Contemporary
    Physics. 19, No. 5 (1978),469-86.

Hooper, A. "Fast Ionic Conductors." Contemporary
    Physics. 19, No. 2 (1978),147-68.

Kittel, Charles. Introduction to Solid State
    Physics. New York: John Wiley and Sons, Inc.,
    1976.

Lidiard, Dr. Alan B. "Ionic Conductivity." Encyclo-
    pedia of Physics. Ed. S. Flugge. Berlin:
    Springer-Verlag, 1957. XX,246-348.

Mooney, J. B. "Some Properties of Single Crystal
    Lanthanum Trifluoride." Infared Physics, 6
    (1966), 153-57.

Smith, Michael K. Dipolar Defects in Rare-Earth
    Doped Alkaline-Earth Fluorides. Report to the
    Trident Scholar Committee. Annapolis, Md.:
    U. S. Naval Academy, 1979.